A Spin Transition Molecular Material with a Wide Bistability Domain

Yann Garcia,*[a, d] Jacques Moscovici,[b, c] Alain Michalowicz,[b, c] Vadim Ksenofontov,[a] Georg Levchenko,[a] Georges Bravic,[d] Daniel Chasseau,[d] and Philipp Gütlich*[a]

Dedicated to Professor Karl Wieghardt on the occasion of his 60th birthday

Abstract: [Fe(hyptrz)$_3$](4-chloro-3-nitrophenylsulfonate)$_2\cdot 2H_2O$ (**1**; hyptrz = 4-(3′-hydroxypropyl)-1,2,4-triazole) has been synthesized and its physical properties have been investigated by several physical techniques including magnetic susceptibility measurements, calorimetry, and Mössbauer, optical, and EXAFS spectroscopy. Compound **1** exhibits a spin transition below room temperature, together with a very wide thermal hysteresis of about 50 K. This represents the widest hysteresis loop ever observed for an Fe^{II}-1,2,4-triazole spin transition material. The cooperativity is discussed on the basis of temperature-dependent EXAFS studies and of the structural features of a Cu^{II} analogue. The EXAFS structural model of (**1**) in both spin states is compared to that obtained for a related material whose spin transition occurs above room temperature. EXAFS spectroscopy suggests that 1,2,4-triazole chain compounds retain a linear character whatever the spin state of the iron(II).

Keywords: chain structures · EXAFS spectroscopy · iron · spin crossover · 1,2,4-triazole

Introduction

Iron(II) spin transition (ST) materials are probably among the most fascinating molecular objects in transition metal chemistry, their spin state being able to be triggered by temperature, pressure, and light.[1–3] The origin of the phenomenon is molecular, but the shape of the temperature dependence of the high-spin (HS, S = 2) molar fraction (γ_{HS} vs T), called the ST curve, is dependent on intermolecular interactions.[1] The more pronounced these interactions are, the steeper the ST curve. The thermally induced transitions between low-spin (LS, S = 0) and HS states may also occur with a hysteresis effect, which confers a memory effect on the system.[4] The fast developments in advanced electronic technology require stable compounds showing bistability behavior on the molecular scale.[4, 5] The use of such materials as molecularly based memory devices and displays is currently being assessed by industrial organizations.[2, 4] This type of application requires abrupt spin transitions at room temperature, with broad thermal hysteresis as well as an associated thermochromic effect.[4, 5] Although cooperative spin transitions have been observed in several monomeric compounds, it is believed that cooperative effects may be favored in cases in which these sites are covalently linked by conjugated ligands.[2] For the resulting polymeric compounds, the molecular distortions involved in the ST might be efficiently distributed throughout the whole crystal lattice through these ligands. The interactions may also be improved by hydrogen-bonding interactions and/or by $\pi-\pi$ stacking orderings.[6–8] Thermal hysteresis has been observed for one-dimensional polymeric Fe^{II}-1,2,4-triazole ST compounds, along with pronounced thermochromic effects.[9–16] Most of these compounds have the general formula [Fe(4-R-1,2,4-triazole)$_3$](anion)$_2\cdot n H_2O$, where n stands for the number of non-coordinated water molecules. So far, no single crystal suitable for X-ray diffraction has been

[a] Dr. Y. Garcia,[+] Prof. Dr. P. Gütlich, Dr. V. Ksenofontov, Dr. G. Levchenko[++]
Institut für Anorganische Chemie und Analytische Chemie
Universität Mainz, Staudingerweg 9, 55099 Mainz (Germany)
Fax: (+49) 6131-3922990
E-mail: garcia@chim.ucl.ac.be, p.guetlich@uni-mainz.de

[b] Dr. J. Moscovici, Prof. Dr. A. Michalowicz
Groupe de Physique des Milieux Denses
Université Paris XII, Avenue du Général de Gaulle
94010 Créteil Cedex (France)

[c] Dr. J. Moscovici, Prof. Dr. A. Michalowicz
Laboratoire d'Utilisation du Rayonnement Electromagnétique
Université Paris Sud, 91405 Orsay Cedex (France)

[d] Dr. Y. Garcia,[+] Dr. G. Bravic, Prof. Dr. D. Chasseau
Groupe des Sciences Moléculaires, ICMCB-CNRS
Avenue du Dr. A. Schweitzer, 33608 Pessac Cedex (France)

[+] Present address:
Department of Chemistry, Université Catholique de Louvain
Place L. Pasteur 1, 1348 Louvain-la-Neuve (Belgium)
Fax: (+32) 1047-2330

[++] Present address:
A. A. Galkin, Donetsk Physical-Technical Institute
R. Luxemburg 72, 83114 Donetsk (Ukraine)

  0947-6539/02/0821-4992 $ 20.00+.50/0

obtained. It has, however, been possible to obtain structural information from EXAFS (X-ray absorption fine structure) at the iron K edge[17–23] and WAXS (wide angle X-ray scattering)[24] spectra. The structure of these materials consists of chains in which the neighboring iron atoms are linked by triple N^1,N^2-1,2,4-triazole bridges.[17] This has been confirmed in the crystal structures of related Cu^{II} compounds.[19, 25] Interestingly, these materials also contain non-coordinating water molecules and anions located between the chains.

We recently initiated a research project aiming to control the ST properties of these materials in order to be able to propose suitable candidates for practical applications. The goal was that both cooperative effects and transition temperature should be controllable in a rational way, in order to obtain wide hysteresis loops around the room temperature region. We decided to favor the formation of hydrogen bonds in the lattice through the introduction of a hydroxyl group on the substituent of the triazole ligand (position 4) and by the introduction of several substituents capable of hydrogen-bonding interactions on the anion, keeping to the idea of increasing intermolecular interactions between polymeric chains. No chain compound of sufficiently large hysteresis has so far been obtainable, however, the hysteresis width typically being around 10 K.[13–16] However, the title compound of the formula [Fe(hyptrz)$_3$](4-chloro-3-nitrophenylsulfonate)$_2\cdot 2H_2O$ (**1**; hyptrz = 4-(3′-hydroxypropyl)-1,2,4-triazole) displays behavior unprecedented in this family of chain compounds, with a very wide thermal hysteresis loop below room temperature. This paper reports on a detailed investigation of this fascinating material. The single-crystal X-ray structure of the related Cu^{II} compound, [Cu(hyptrz)$_3$](4-chloro-3-nitrophenylsulfonate)$_2\cdot H_2O$, is also reported.

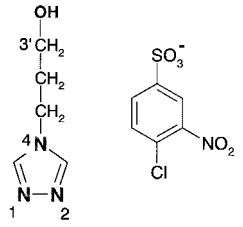

Results of Physical Studies

Magnetic measurements: The temperature dependence of the molar magnetic susceptibility is displayed in Figure 1 in the form of a $\chi_M T$ versus T plot, χ_M being the molar magnetic susceptibility corrected for diamagnetic contributions and T the temperature. At room temperature, $\chi_M T$ is equal to 3.35 $cm^3 mol^{-1} K$, which indicates Fe^{II} ions being present in the HS state. As T is lowered, $\chi_M T$ initially remains constant down to 170 K and then decreases rapidly in the 120–90 K temperature range, reaching a value of 1.03 $cm^3 mol^{-1} K$ at 90 K. Below this T, $\chi_M T$ shows a plateau with a value of 0.89 $cm^3 mol^{-1} K$ at 40 K, and finally falls to 0.36 $cm^3 mol^{-1} K$ at 4.2 K. As T is increased, $\chi_M T$ increases gradually up to 150 K and then much more rapidly above this temperature, to match the starting $\chi_M T$ values. The transition temperatures (the temperatures at which 50 % of LS and HS molecules are present) are $T_{1/2}\downarrow = 120$ K and $T_{1/2}\uparrow = 168$ K. Thus, an extremely large thermal hysteresis loop of 48 K is observed,

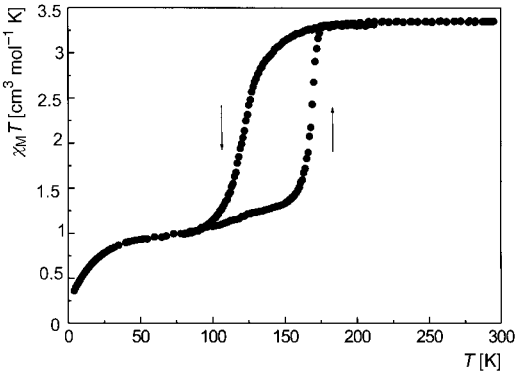

Figure 1. Temperature dependence of $\chi_M T$ for **1**, in both the cooling and the warming modes.

centered at 144 K. This hysteresis is retained over successive thermal cycles. The HS → LS transition is not complete at low temperature. The fall in $\chi_M T$ below 40 K is due to the zero-field splitting of the HS Fe^{II} ions, and the preferred Boltzmann population of the lowest levels with decreasing temperatures. The magnetic properties of compound **1** were also investigated under pressures of up to ≈2 kbar; the result is presented in Figure 2. On comparing the ambient pressure curve of Figure 1 with that of Figure 2, one notices that the

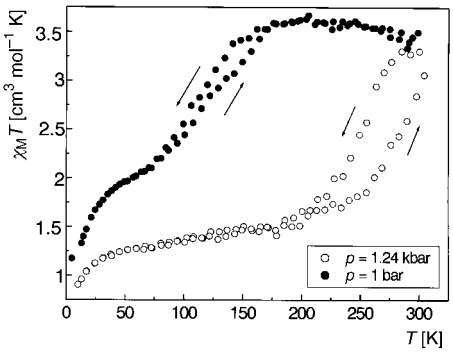

Figure 2. Temperature dependence of $\chi_M T$ for **1**, in both the cooling and the warming modes, at 1 bar (●) and at 1.24 kbar (○).

large hysteresis width has disappeared. This behavior is most probably due to the interaction between the silicon oil used as a pressure-transmitting medium and compound **1**. On application of pressure, a parallel shift towards higher temperatures was observed. At 1.24 kbar, a wider hysteresis width is recovered below room temperature, with $T_{1/2}\downarrow = 250$ K and $T_{1/2}\uparrow = 290$ K, and at 2.3 kbar the compound is in the LS state at room temperature. Thus a shift of 100 K per kbar is observed. On release of pressure, the initial curve is recovered, showing that there is no chemical degradation and no relaxation to another state.

Compound **2** was obtained by heating **1**, under nitrogen, up to the temperature corresponding to complete dehydration as determined from thermogravimetric measurements (423 K). The temperature dependence of $\chi_M T$ shows a very gradual decrease upon cooling ($\chi_M T^{293} = 3.26$ $cm^3 mol^{-1} K$, which indicates HS Fe^{II} ions) down to 50 K, at which a rapid drop is

  0947-6539/02/0821-4993 $ 20.00+.50/0

observed. This behavior probably indicates an antiferromagnetic interaction between HS Fe^{II} ions within the chain.

Optical detection of the spin state: Compound **1**, which presents a thermochromic effect (from white to pink) upon cooling, was studied optically. The presence of a very wide hysteresis loop, retained over successive thermal cycles, was confirmed by this technique. The optical response of **2** was also investigated down to 90 K; no change of signal was observed.

Mössbauer spectroscopy: Mössbauer spectra of **1** were recorded from room temperature down to 55 K. Selected spectra are displayed in Figure 3, and detailed values of the Mössbauer parameters deduced from least-squares fitting procedures are listed in Table 1. At room temperature, the spectrum shows a symmetrical doublet, indicating Fe^{II} ions in the HS state. Upon cooling, an additional doublet characteristic of the LS state of the Fe^{II} ion appears at $\approx$180 K. Its relative intensity increases very rapidly as T decreases between 150 and 120 K (see Figure 3). At 120 K, the LS doublet is resolved and shows a noticeable splitting. This splitting indicates that the local environment of the LS Fe^{II} ions is not cubic. At 55 K, the spectrum reveals the presence of $\approx$16 % of HS Fe^{II} ions, confirming the incomplete character of the spin transition. Upon heating, the spectra remain essentially similar up to 150 K, at which point a dramatic increase in the intensity of the HS doublet is observed. It is interesting to compare the spectra recorded at the same temperature (150 K) upon cooling and heating, which clearly reflect a memory effect. The ST curve deduced from ^{57}Fe Mössbauer spectroscopy closely resembles that in the magnetic curve (see Figure 4).

Table 1. ^{57}Fe Mössbauer parameters [mm s^{-1}] for **1**.[a]

T [K]	δ(LS)	ΔE_Q(LS)	$\Gamma/2$(LS)	δ(HS)	ΔE_Q(HS)	$\Gamma/2$(HS)	A_{HS} [%]
300				0.943(2)	2.667(4)	0.27(1)	100
250 ↓				0.977(2)	2.907(4)	0.27(1)	100
200 ↓				1.000(2)	3.039(4)	0.24(1)	100
150 ↓	0.413(2)	0.281(2)	0.25(1)	1.025(1)	3.189(4)	0.27(1)	90.0
120 ↓	0.413(2)	0.291(2)	0.26(1)	1.037(2)	3.270(4)	0.28(1)	32.7
81 ↓	0.419(2)	0.298(2)	0.26(1)	1.055(2)	3.330(4)	0.31(1)	18.5
56 ↓	0.422(2)	0.298(2)	0.27(1)	1.059(2)	3.348(4)	0.30(1)	15.6
55 ↓	0.421(2)	0.299(2)	0.27(1)	1.066(2)	3.336(4)	0.31(1)	16.2
70 ↑	0.420(2)	0.298(2)	0.28(1)	1.055(2)	3.340(4)	0.32(1)	16.8
100 ↑	0.416(2)	0.296(2)	0.26(1)	1.051(2)	3.330(4)	0.30(1)	19.0
120 ↑	0.413(2)	0.292(2)	0.31(1)	1.047(2)	3.302(4)	0.27(1)	21.9
150 ↑	0.409(2)	0.287(2)	0.26(1)	1.033(2)	3.257(4)	0.30(1)	25.6
169 ↑	0.404(2)	0.282(2)	0.25(1)	1.020(2)	3.180(4)	0.28(1)	43.0
180 ↑	0.444(2)	0.278(2)	0.23(1)	1.010(2)	3.101(4)	0.27(1)	95.8

[a] δ = isomer shift relative to α iron, ΔE_Q = quadrupole splitting, $\Gamma/2$ = half-width of the lines, A_{HS} = area fraction of the HS doublets. Statistical standard deviations are given in parentheses. The arrows indicate the temperature mode: ↓ for cooling and ↑ for heating.

Calorimetric measurements: The DSC curve for increasing temperature from 140 to 220 K is represented in Figure 5. This curve shows an endothermic peak around 172 K. This peak is obviously related to the LS → HS transition for **1** detected in

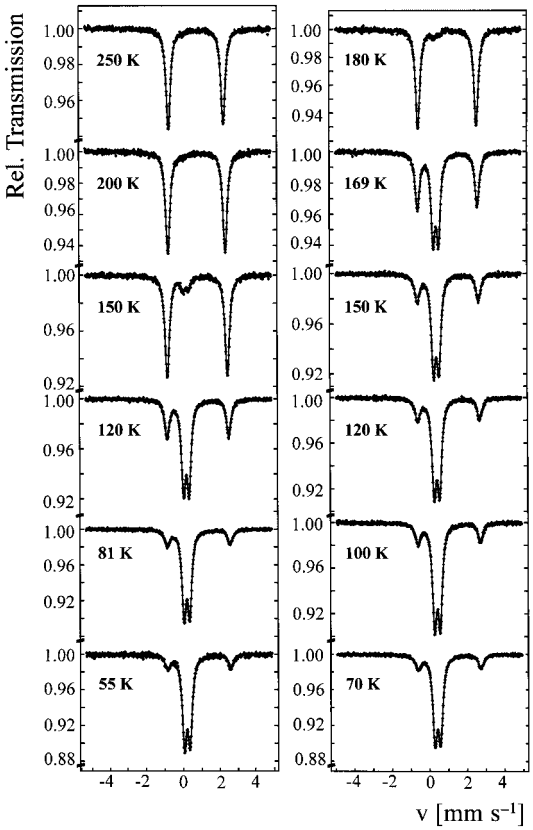

Figure 3. Selected ^{57}Fe Mössbauer spectra for **1** as a function of temperature. Cooling mode (left), heating mode (right).

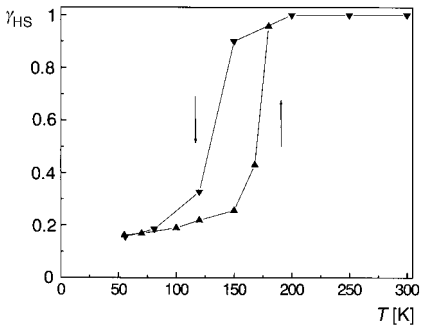

Figure 4. Temperature dependence of the HS molar fraction for **1** as deduced from ^{57}Fe Mössbauer spectroscopy. The points (▼) and (▲) refer to the cooling and heating modes respectively. The line is used as a guide for the eyes.

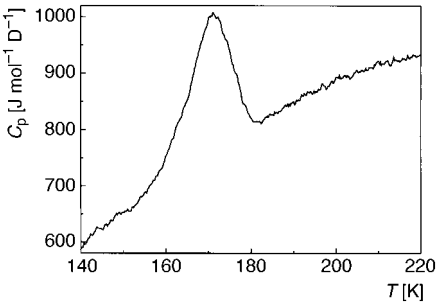

Figure 5. DSC for **1** in the 140–240 K temperature range.

0947-6539/02/0821-4994 $ 20.00+.50/0 *Chem. Eur. J.* **2002**, *8*, No. 21

Mössbauer, magnetic, and optical studies. It is indicative of a first order phase transition. The thermodynamic parameters have been evaluated as $\Delta H = 7.3\ kJ\,mol^{-1}$ and $\Delta S = 42.4\ J\,mol^{-1}\,K^{-1}$. The experimentally measured entropy variation can be accounted for by an electronic contribution, $Rln5 = 13.4\ J\,mol^{-1}\,K^{-1}$, and a vibrational contribution.[1] DSC curves were also recorded for **2**, but no signal was observed upon cooling.

EXAFS: X-ray absorption spectra of **1** were recorded between 280 K and 40 K, including within its bistability domain, both in the LS and HS states. For comparison, X-ray absorption spectra of $[Fe(Htrz)_2trz](BF_4)$ (**3**; Htrz = 4H-1,2,4-triazole; trz = triazolato), between 300 and 400 K, including in its bistability domain (360 K, LS and HS states) were also recorded. Some corresponding $k\chi(k)$ EXAFS spectra are presented in Figure 6a, and the Fourier transform (FT) moduli of **1** (Figure 6b) and **3** (Figure 6c) in both spin states are superimposed in order to present the local structure changes during the spin transition qualitatively. These spectra are composed of five main peaks. The first peak is assigned to the octahedral coordination sphere FeN_6, and the intermediate peaks to the carbon and nitrogen atoms of the triazole rings overlapping with the Fe–Fe signal around 3.5 Å, the former not being clearly separated.[17] The last one, around 7 Å, indicated by an arrow, corresponds to the multiple scattering path Fe–Fe–Fe.[17, 18] In this work, we focus on a qualitative discussion of the FeN_6 peak and of the multiple scattering Fe–Fe–Fe signals. Full discussion of the EXAFS structure needs full multiple scattering ab initio calculations and was beyond the scope of this study, as this topic has been addressed for similar compounds.[17–19, 21, 23]

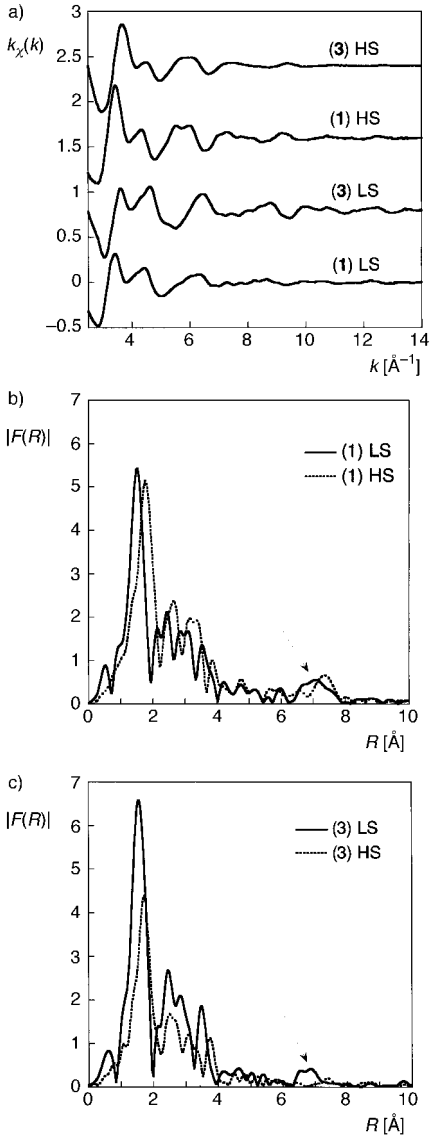

Figure 6. a) EXAFS spectra of **1** in both the HS and LS states at 150 K and of **3** at 150 K and 360 K. b) Modulus of the FT of the experimental EXAFS spectra for **1** at 150 K in the LS state (——) and HS state (- - - -). c) Modulus of the FT of the experimental EXAFS spectra for **3** at 360 K in the LS state (——) and HS state (- - - -).

In Figure 6b and c, a shift to higher distances is observed for the dotted spectrum relative to the HS state with increasing temperature. This shift corresponds to the expected elongation of Fe–N bond lengths for the Fe^{II} ion on going from LS → HS. We also observe a slight decrease in the modulus of the FT signal on going from LS → HS states for **1**. The distance variation is similar to that observed in previously studied compounds of this family, such as for **3** (Figure 6c).[17, 18] In contrast, the amplitude variation through the ST is different for **1** and **3**. In the first compound, the decrease in amplitude is very small, whereas strong decreases in both the FeN_6 and the Fe–Fe–Fe peaks are observed for **3**. It is worth mentioning that the very small but noticeable 7 Å peak observed in the spectrum of **3** in the HS state was not observed in our previous papers.[17, 18] We could not rule out that this peak had indeed been present but masked by the noise level.[17] In this work, we present new measurements in which the experimental statistics were improved in order to check carefully for the presence or the absence of this signal above the noise level. These qualitative observations are quantified for the FeN_6 signal by least squares fitting of the filtered EXAFS spectra. The results are shown in Table 2 and in Figure 7.

The Fe–N distances of 1.99 and 2.19 Å are typical for Fe^{II} ions in the LS and HS states, respectively. The Fe–N bond lengthens by 0.20(1) Å during the ST and coincides with the values found for other Fe^{II} linear chain compounds with 4-R-1,2,4-triazole compounds as ligands. It is found, for instance, as ≈0.18 Å for **3**[17] or as 0.23 Å for $[Fe(NH_2trz)_3](NO_3)_2$ (NH_2trz = 4-amino-1,2,4-triazole).[20] The HS molar fraction deduced from EXAFS fitting of compounds **1** and **3** around their ST are plotted in Figure 7a and b, respectively. These results qualitatively confirm the HS molar fractions obtained by Mössbauer spectroscopy for **1** (Table 1) and for **3**.[10] However, it seems that EXAFS underestimates the HS fraction in the LS region for compound **1**. As measured by Mössbauer spectroscopy at 150 K, γ_{HS} is equal to 0.9 and 0.25 in the cooling and in the heating modes, respectively, and the corresponding EXAFS values are ≈1.0 and ≈0.3. It is clear that EXAFS is not the most accurate way to measure the HS/LS ratio, but it does, however, enable one to characterize the vibrational movements around the Fe^{II} central ions directly by the cooperative dependence of the Debye–Waller factor, and for a polycrystalline sample it represents the only way to characterize the structural alignment of these Fe^{II} ions by

  0947-6539/02/0821-4995 $ 20.00+.50/0

Table 2. Fitting of the first Fe coordination sphere of the EXAFS data for **1** at different temperatures. The R value was determined in the LS state at 40 K and in the HS state at 320 K. These values were fixed in order to improve the accuracy for the fitting of N and σ.

T [K]	Spin state	N[a]	σ [Å][b]	R [Å][c]	ΔE_0 [eV][b]	ρ [%]
40 ↑	LS	5.7(3)	0.0059(6)	1.99(2)	−3.0(1.0)	2.0
	HS	0.3	0.059	2.19	−3.0	
70 ↑	LS	5.5(3)	0.0058(6)	1.99	−2.8(1.0)	1.4
	HS	0.5	0.0058	2.19	−2.8	
90 ↑	LS	5.4(5)	0.0059(9)	1.99	−1.6(1.0)	1.8
	HS	0.6	0.0059	2.19	−1.6	
100 ↑	LS	5.2(4)	0.006(1)	1.99	−2.1(1.0)	3.5
	HS	0.8	0.006	2.19	−2.1	
110 ↑	LS	5.1(5)	0.0059(9)	1.99	−3.4(1.1)	1.7
	HS	0.9	0.0059	2.19	−3.4	
130 ↑	LS	4.7(5)	0.0059(11)	1.99	−1.9(1.2)	2.5
	HS	1.3	0.0059	2.19	−1.9	
150 ↑	LS	4.3(5)	0.0058(10)	1.99	−2.3(1.4)	3.9
	HS	1.7	0.0058	2.19	−2.3	
168 ↑	LS	0.6(5)	0.0058(9)	1.99	−0.7(1.2)	9.0
	HS	5.4	0.0058	2.19	−1.6	
175 ↑	LS	0.0(5)	0.0061(7)	1.99	−3.1(1.0)	8.9
	HS	6.0	0.0061	2.19	−3.1	
280 ↑	LS	0.0(5)	0.0068(7)	1.99	−1.4(1.0)	9.4
	HS	6.0	0.0068	2.19(2)	−1.4	
150 ↓	LS	0.0(5)	0.0061(7)	1.99	−0.26(49)	9.7
	HS	6.0	0.0061	2.19	−0.26	
130 ↓	LS	0.85(49)	0.0056(11)	1.99	−0.5(1.3)	9.0
	HS	5.15	0.0056	2.19	−0.5	
120 ↓	LS	2.2(4)	0.0063(12)	1.99	−4.3(1.7)	9.9
	HS	3.8	0.0063	2.19	−4.3	

[a] $N_{LS} + N_{HS} = 6$. [b] Same value in both states. [c] Values of R fixed to those fitted at 40 K (LS) and 280 K (HS).

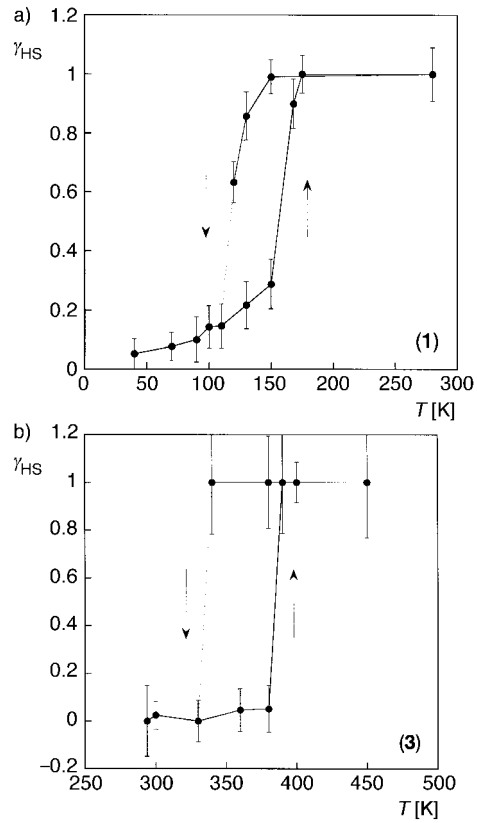

Figure 7. Temperature dependence of the HS molar fraction, deduced from EXAFS spectroscopy: a) for compound **1**, and b) for compound **3**. The dotted lines are guides for the eyes.

examination of the 7 Å multiple scattering FT peak. A quantitative study of the temperature dependence of the Debye–Waller factors is presented in Figure 8a and b for compounds **1** and **3**, respectively. These results confirm those

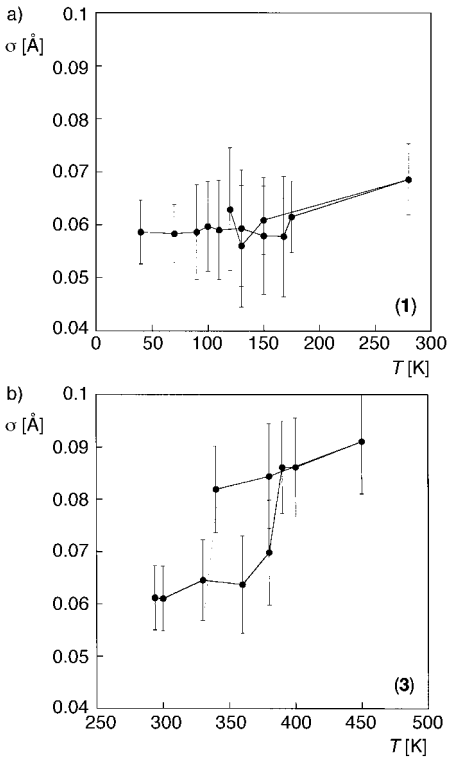

Figure 8. Debye–Waller factor vs temperature: a) for compound **1**, and b) for compound (**3**). The dotted line is a guide for the eyes.

already published elsewhere.[23] For **1**, there is no measurable variation of the Fe–N Debye–Waller factor through the transition. This is a new and unexpected result in comparison to the case of **3**, in which we confirm the already observed important Debye–Waller variation. One may notice that in the LS state the amplitude of the FeN_6 peak of **1** is low compared to the corresponding signal in compound **3**. This is confirmed quantitatively by the Debye–Waller factor values in Table 2: for compound **1** in the LS state $\sigma_{FeN_6} = 0.058$ Å, and for compound **3** $\sigma_{FeN_6} = 0.061$ Å. The amplitude of the 7 Å multiple scattering peak qualitatively follows the same behavior: as already mentioned for **1**, this peak remains in both spin states when the temperature is sufficiently low. At room temperature it has been shown that the 7 Å peak disappears, while it is still intense for **3**.

X-ray crystal structure of [Cu(hyptrz)$_3$](4-chloro-3-nitrophenylsulfonate)$_2 \cdot H_2O$: An X-ray crystallographic structure determination of [Cu^{II}(hyptrz)$_3$](4-chloro-3-nitrophenylsulfonate)$_2 \cdot H_2O$ (**4**) was carried out at 293 K (Figure 9).[26] Each copper atom is coordinated to six hyptrz ligands, half of them originating from the other triazole moieties by centrosymmetry. Each ligand (x) is in this way linked to Cu(1) through the nitrogen atoms N(x1) and to Cu(2) through N(x2), and are thus bidentate. These bonds are repeated three times in the a direction of the unit cell, thus forming a chain in which each

0947-6539/02/0821-4996 $ 20.00+.50/0 *Chem. Eur. J.* **2002**, *8*, No. 21

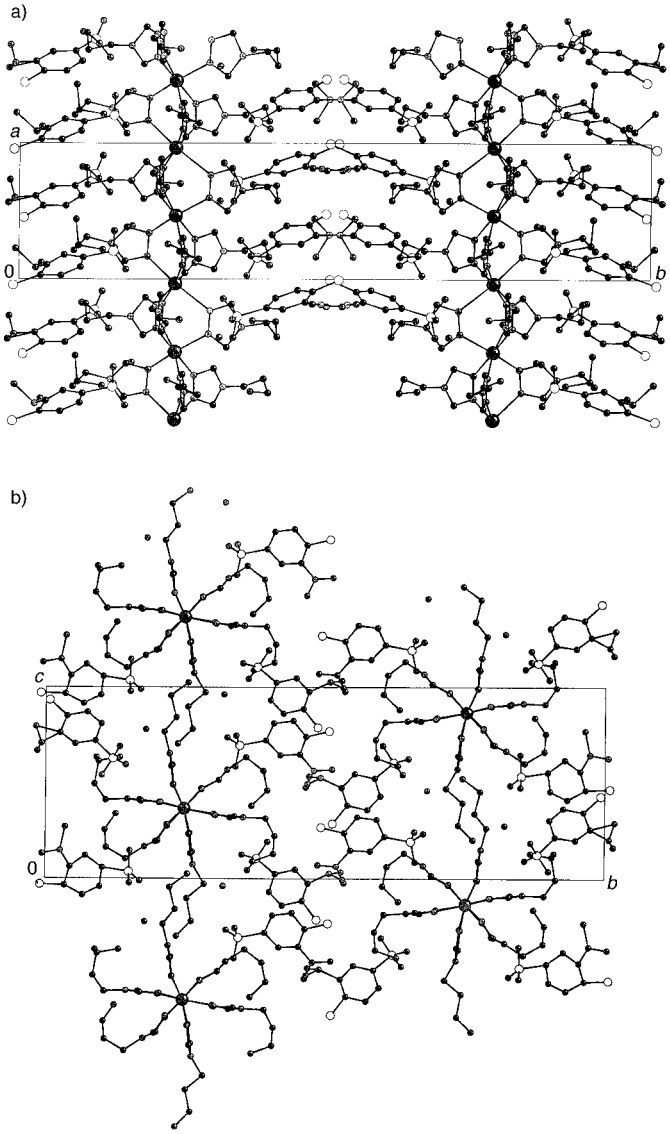

Figure 9. View of the crystal structure of **4**: on the (*ab*) plane (top, a), and the (*bc*) plane (bottom, b).

polymeric unit has half a cell parameter length in this direction: that is, 3.962 Å. The medium planes of the triazole groups of a given unit are superimposed by successive rotations of 117, 109, and 134° around the *a* direction. Two of the hydroxypropyl substituents adopt a bent conformation as indicated by the torsional angles N(14)-C(16)-C(17)-C(18) 51.8(4)° and N(34)-C(36)-C(37)-C(38) 57.4(5)°, whereas the third substituent has an elongated conformation with N(24)-C(26)-C(27)-C(28) −173.6(3)°.

The two copper atoms have octahedral surroundings but the coordination octahedra are quite different. We consider here three different types of Cu–N bonds in terms of their length: short (2.0 ± 0.1 Å), medium (2.2 ± 0.1 Å), and long (2.4 ± 0.1 Å). The Cu(1) octahedron has four short bond lengths Cu(1)–N(11) and Cu(1)–N(21) and two long bond lengths Cu(1)–N(31) and is thus elongated along the vertices N(31) and N(31)[1]. The Cu(2) octahedron has four medium bond lengths Cu(2)–N(12) and Cu(2)–N(22) and two short bond lengths Cu(2)–N(32) and is thus compressed along the vertices N(32) and N(32)[2]. The angle between the N(31)-N(31)[1] and N(32)-N(32)[2] axes of these two octahedra is equal to 70.7°.

The cations and the anions form successive layers stacking along the *b* direction of the unit cell (Figure 9b). The neighboring columns are thus closer along the [001] row (12.69 Å) than along the [011] row (19.42 Å) and interchain contacts only exist along the first direction. Most important is the hydrogen bond between the $H_2O(4)$ water molecule and the hydroxyl groups O(39) (2.769(5) Å) and O(29) (2.670(5) Å). We can also note anion–cation interactions between terminal hydroxyl groups and sulfonate anions: for instance, O(19)···O(811) (2.737(4) Å) and O(39)···O(813) (2.666(5) Å).

Discussion and Conclusion

Compound **1** represents a novel ST material showing a very wide and fully reproducible hysteresis loop (48 K), centered around 145 K. This compound shows the widest hysteresis loop ever reported for an Fe^{II}-1,2,4-triazole chain compound. This hysteresis is an intrinsic property of the system and is not accompanied by any solvent removal. The transition is, however, not complete, ≈16% of the Fe^{II} ions remain in the HS state at low temperature. This behavior could be attributable to the presence of HS Fe^{II} external ions of the chains, whatever the temperature, as a consequence of their coordination to water molecules.[31] The presence of defects in the material, introduced—for instance—by chains of different lengths, could also be put forward to explain this behavior.

The hysteresis loop may have several origins such as, for instance, a local structural change around the Fe^{II} ion or a crystallographic phase transition, which could be favored by a twist of the chains, on going from LS to HS. These aspects motivated us to perform structural studies on this type of materials. In the absence of suitable single crystals for X-ray diffraction, the very first EXAFS results on Fe^{II}-1,2,4-triazole chain compounds were reported in 1994,[20] focusing only on the structural changes of the first coordination sphere FeN_6 due to the spin transition. EXAFS characterization of the structure beyond the immediate neighbors was published a year later.[17] The main result in this paper was the detection of an EXAFS signal at an exceptionally long distance (around 7 Å), which was positively analyzed as the signature of the double Fe···Fe distance, only visible if the Fe^{II} chain is aligned.[21, 23, 32] For all compounds of this series, this signal was always observed in the LS state but was doubtful in the HS state. For compounds with ST above room temperature, such as $[Fe(Htrz)_2trz](BF_4)$ (**3**), the Fe–Fe–Fe alignment EXAFS signature was difficult to derive because of the high noise level, if present in the HS state. This is why a misalignment in the HS state was put forward to account for this behavior. An alternate zigzag structure of the chain was also proposed,[17] and strongly supported later by WAXS studies.[24] This change in the chain conformation was presumed to be responsible for the huge hysteresis observed, by assuming a structural reorganization upon the spin transition. Up to now, however, the structural character of

  0947-6539/02/0821-4997 $ 20.00+.50/0

the chains in the HS state (linear or bent) is still a matter of debate, as a linear twisted configuration could also account for the huge hysteresis observed. Here we discuss the Fe – Fe – Fe alignment by focusing on a compound existing in the HS state down to 140 K (**1**) and compare our EXAFS results to those obtained for compound **3**.[17] Our current results show that the Fe – Fe – Fe alignment in compound **1** is preserved across the spin transition. In the case of compound **3**, powder diffraction spectra recently recorded in the LS and HS states by use of synchrotron radiation facilities proved to be similar, indicating no crystallographic phase transition.[33]

The temperature dependence of the Debye – Waller factor deduced by EXAFS spectroscopy of a ST compound was studied for the mononuclear compound $[Fe(bpp)_2](BF_4)_2$ (bpp = 2,6-bis(pyrazol-3-yl)pyridine)[34] undergoing a discontinuous transition around 180 K.[35] The observed jump of the Debye – Waller factor at the ST temperature was, however, neither commented on nor physically explained by the authors. For compound **1**, we observe no significant variation in the FeN_6 Debye – Waller coefficient, whereas for compound **3**, $\Delta\sigma^2 = 3.6\ 10^{-3}$ Å^2. EXAFS Debye – Waller coefficients are related to a combination of structural disorder (site distortion) and thermal vibrations. Both phenomena contribute to the width of the radial distribution function. In compound **3**, we observe an important increase in this parameter across the ST, consistent with the transition between an Fe^{II} d^6 LS non-degenerate octahedral $^1A_{1g}$ electronic state to an Fe^{II} d^6 HS degenerate $^5T_{2g}$ state. Large Jahn – Teller distortions are usually observed for E_g degenerated states, such as in d^9 complexes. These d^6 HS systems, however, can also undergo small distortions. Both structure and vibrational states can be affected, but the geometrical distortion of the Fe^{II} HS octahedral site was found to be smaller than the EXAFS resolution ($\Delta_r < 0.1$ Å). For this reason, the observed EXAFS Debye – Waller factor increase through the ST can be assigned either to static or to dynamic distortion without any possibility of discriminating between the two distortions.

In contrast, the Debye – Waller factor of compound **1** seems to be unaffected by the spin transition. This unexpected behavior should be related to the vibrational entropy changes of these two compounds: $\Delta S_{vib} = 66$ J mol^{-1} K^{-1} for compound **3**[10] and $\Delta S_{vib} = 29$ J mol^{-1} K^{-1} for compound **1**. Calorimetric measurements and EXAFS Debye – Waller coefficients lead to the same conclusion: at the same temperature, the LS compound **1** is less rigid than compound **3**. This rigidity develops smoothly versus T for compound **1**, without any apparent jump in the ST, whereas compound **3** undergoes a pronounced increase in its rigidity during the transition. Finally, it appears that the exceptional hysteresis width observed for compound **1** is related neither to a pronounced local change in the thermal vibrations, nor to a change in the alignment of the Fe^{II} ions. We believe that this hysteresis is the result of strong cooperative effects due to a link between the Fe^{II} chains. In an attempt to check this hypothesis, we were able to grow single crystals of the relative Cu^{II} compound, $[Cu(hyptrz)_3]$(4-chloro-3-nitrophenylsulfonate)$_2 \cdot H_2O$ (**4**) and to solve its crystal structure. This material shows a powder diffraction pattern very similar to that of **1** and is assumed to be isostructural, as observed in other studies of related molecularly based 1,2,4-triazole materials.[36] The molecular organization of this compound, however, differs from that observed for $[Cu(hyetrz)_3](ClO_4)_2 \cdot 3H_2O$ (hyetrz = 4-2′-hydroxyethyl-1,2,4-triazole),[19] in which the linear chains were found to be "isolated" from each other. Here, there exist direct links between the linear chains through hydrogen bonds. In addition, the anion and the water molecules are involved in an extensive hydrogen-bonding network, and stacking interactions are also found. This molecular organization could well be the source of the huge cooperative effects developed by compound **1**.

In terms of potential practical applications, this material could be proposed as a memory effect pressure sensor. This hysteresis loop with a wide range of bistability, however, is situated too far below room temperature to be directly usable at ambient temperature and pressure. The application of external pressure should get round this difficulty, as it is now established that pressure can stabilize the LS state and shift the hysteresis loops of such Fe^{II} 1,2,4-triazole chain compounds without significant modification.[15, 16] It has, for instance, been observed that the ST curves of $[Fe(hyptrz)_3]$(4-chlorophenylsulfonate)$_2 \cdot H_2O$ could be shifted from 174 to 325 K by pressure, without significantly altering the shape and the width of the hysteresis loop.[16] Astonishingly, the magnetic properties of **1** could not be recovered in our pressure cell at 1 bar. This observation could be due to the fact that iron(II)-1,2,4-triazole chain compounds are known to be porous and can therefore easily incorporate solvent of different shape and volume.[15] This points to a dramatic influence of the silicon oil used as the pressure-transmitting medium on the magnetic properties of such sensitive molecular compounds, a result that has also been observed in other possible porous ST molecular materials.[37] It is also worthwhile mentioning that, if **1** is prepared in DMF, a violet LS compound is obtained.

The non-coordinated water molecules assumed to be located between the chains play a key role for compound **1**. Removal of these solvent molecules by complete dehydration gives rise to a new compound (**2**), which does not show a ST any more. This behavior has already been observed for another polymeric ST compound: $[Fe(4,4'\text{-bis-1,2,4-triazole})_2(NCS)_2] \cdot H_2O$, which presents a very abrupt ST around 134 K with a thermal hysteresis of 25 K, whereas its dehydrated form is HS over the whole temperature range.[38] In this material, non-coordinated water molecules stand between two-dimensional layers, linked by hydrogen-bonding interactions to the peripheral nitrogen atoms of the triazole ligands. This behavior is actually not typical for polymeric ST compounds, as the linear chain $[Fe(hyetrz)_3](ClO_4)_2 \cdot n H_2O$ ($n = 0$, 2) retains a discontinuous ST whatever the solvent molecule content.[14]

Experimental Section

Syntheses: The hyptrz ligand was prepared as previously described.[16] The $[M(H_2O)_6]$(4-chloro-3-nitrophenylsulfonate)$_2$ (M = Fe^{II}, Cu^{II}) salts were obtained by treatment of aqueous solutions of 4-chloro-3-nitrophenylsul-

0947-6539/02/0821-4998 $ 20.00+.50/0 *Chem. Eur. J.* **2002**, *8*, No. 21

fonic acid and $FeCl_2 \cdot 4H_2O$ or $CuCl_2 \cdot 2H_2O$ according to the procedure given in ref. [15]. Compound **1** was synthesized under nitrogen atmosphere as follows: $[Fe(H_2O)_6](4\text{-chloro-3-nitrophenylsulfonate})_2$ (0.75 g, 1.2 mmol) in methanol (35 mL), together with a few mg of ascorbic acid was heated at 65 °C and added to hyptrz (0.45 g, 3.5 mmol) in methanol (5 mL). The mixture was stirred overnight at room temperature, during which a white precipitate was formed. It was filtered, washed with methanol, and dried in air. IR (KBr): $\tilde{\nu}_a(SO_3^-) = 1287\ cm^{-1}$; elemental analysis calcd (%)for $C_{24}H_{33}N_{11}O_{16}S_2Cl_2Fe$ (**1**): C 34.26, H 3.94, N 16.28, S 6.77, Cl 7.49, Fe 5.90; found C 34.33, H 3.81, N 16.29, S 6.25, Fe 6.11. The number of water molecules of the compound was confirmed by thermogravimetric analysis. $[Fe(Htrz)_2trz](BF_4)_2$ (**3**) was synthesized as described in ref. [10] working in an $EtOH/H_2O$ medium.

Compound **4** was synthesized as follows: hyptrz (0.13 g, 1.02 mmol) in water (5 mL) was added to a green methanolic solution (5 mL) containing $[Cu(H_2O)_6](4\text{-chloro-3-nitrophenylsulfonate})_2$ (0.21g, 0.32 mmol). Crystals slowly formed inside the resulting blue solution at room temperature. IR (KBr): $\tilde{\nu}_a(SO_3^-) = 1287\ cm^{-1}$.

Physical measurements: Infrared spectra were recorded on a Perkin–Elmer Paragon 1000 FT-IR spectrophotometer. The ST was detected optically by the reflectivity of the material at 520 nm, by use of a setup described elsewhere.[39] Thermogravimetric measurements were carried out with a SETARAM apparatus in the 293–400 K temperature range under ambient atmosphere. The differential scanning calorimetry experiments were performed under $He_{(g)}$ atmosphere with a Perkin–Elmer DSC-7 instrument working down to 100 K. The rates of heating and cooling were fixed at 2 K min^{-1}. Details of the experimental procedure are described elsewhere.[40] The magnetic susceptibility measurements were performed with a DSM-8 susceptometer, a MPMS-5S SQUID magnetometer, and a PAR 151 Foner-type magnetometer, working in the 4.2–300 K temperature range. The hydrostatic high-pressure cell with silicon oil as the pressure-transmitting medium has been described elsewhere,[41] with the hydrostaticity having been established in our earlier studies.[15, 16] The pressure was measured with the aid of the known pressure dependence of a superconducting transition of an internal tin manometer. Magnetic data were corrected for magnetization of the sample holder and for diamagnetic contributions, which were estimated from the Pascal constants. X-ray powder patterns were recorded at room temperature on a PHILIPS PW 1710 counter diffractometer with $Cu_{K\alpha}$ radiation. ^{57}Fe Mössbauer measurements were performed on a constant acceleration-type spectrometer with a room-temperature ^{57}Co source (Rh matrix) in transmission geometry and a helium cryostat. All isomer shifts refer to natural Fe at room temperature. The spectra were fitted to Lorentzians with the program MOSFUN,[42] by assuming equal Debye–Waller factors of the HS and LS states at a given temperature. The EXAFS spectra were recorded at LURE, the French synchrotron radiation facility, on the DCI storage ring (1.85 GeV, 300 mA), on the D42 spectrometer, with a Si111 channel-cut monochromator. The detectors were low-pressure ($\approx$0.2 atm) air-filled ionization chambers. Each spectrum is the sum of three recordings in the 7080–8080 eV range (energy steps = 2 eV), including the iron K edge ($\approx$7115 eV). The spectra were recorded at several temperatures by use of a liquid helium cryostat for **1** and an oven for **3**, equipped with a TBT temperature controller. The samples were prepared as homogeneous pellets embedded between two films of Kapton, a polymer transparent to X-rays. The mass ($\approx$50 mg) was calculated in order to obtain an absorption jump at the edge $\Delta\mu x \approx 1.0$, with a total absorption above the edge less than $\mu x \approx 3$. EXAFS data analysis was performed with the programs "EXAFS pour le Mac" and EXAFS98.[43] This standard EXAFS analysis[44] includes linear pre-edge background removal, a smoothing spline atomic absorption energy-dependent procedure, Lengeler–Eisenberger EXAFS spectra normalization,[45] and reduction from the absorption data $\mu(E)$ to the EXAFS spectrum $\chi(k)$ with

$$k = \sqrt{\frac{2m_e}{(\hbar)^2}(E - E_0)} \qquad (1)$$

where E_0 is the energy threshold, taken at the absorption maximum (7120 ± 1 eV). Radial distribution functions $F(R)$ were calculated by Fourier transforms of $k^3 w(k)\chi(k)$ in the 2–14 Å^{-1} range; $w(k)$ is a Kaiser–Bessel apodization window with a smoothness coefficient $\tau = 3$. After Fourier filtering, the first single-shell Fe-6N was fitted, in the 3–14 Å^{-1} range (resolution $\pi/2\partial k = 0.14$ Å) to the standard EXAFS formula, without multiple scattering:

$$k_\chi(k) = -S_0^2 \sum_{i=1.5} \left[\frac{N_i}{R_2^i} |(F\pi,k)| e^{-2\sigma^2 k^2} e^{-\frac{2R_i}{\lambda(k)}} \sin(2kR_i + 2\partial_1(k) + \Psi(k)) \right] \qquad (2)$$

where S_0^2 is the inelastic reduction factor, N is the number of nitrogen atoms at the distance R from the iron center, λ is the mean free path of the photoelectron, σ is the Debye–Waller coefficient, characteristic of the width of the Fe–N distance distribution, $\partial_1(k)$ is the central atom phase shift, and $|(F\pi,k)|$ and ψ(k) the amplitude and phase of the nitrogen backscattering factor. Spherical-wave theoretical amplitudes and phase shifts calculated by the code FEFF were used.[46] Since theoretical phase shifts were used, it was necessary to fit the energy threshold E_0 by adding an extra fitting parameter, ΔE_0, and to introduce two Fe–N distances characteristic of the LS and HS states for **1**. This is why the EXAFS spectra are represented by a sum of two terms, reflecting the mixing of both LS and HS states, even at 4.2 K. The goodness of fit was given by:

$$\rho(\%) = \frac{\sum [k\chi_{exp}(k) - k\chi_{th}(k)]^2}{[k\chi_{exp}(k)]^2} \qquad (3)$$

and the fitting uncertainties were estimated in the standard manner, with the statistical $\Delta\chi^2$.[44c] The experimental error bars were estimated by a classical statistical method.[47]

Acknowledgement

This work was supported by the TMR Research Network ERB-FMRX-CT98–0199 (TOSS), the Fonds der Chemischen Industrie, and the Materialwissenschafliches Forschungszentrum der Universität Mainz. We thank L. Rabardel, T. Maris, and F. Bouamrane for their assistance in the recording of the calorimetric, single-crystal X-ray diffraction, and EXAFS data, respectively, and R. Lapouyade for useful comments.

[1] P. Gütlich, A. Hauser, H. Spiering, *Angew. Chem.* **1994**, *106*, 2109; *Angew. Chem. Int. Ed. Engl.* **1994**, *33*, 2024.
[2] P. Gütlich, Y. Garcia, H. A. Goodwin, *Chem. Soc. Rev.* **2000**, *29*, 419.
[3] P. Gütlich, Y. Garcia, T. Woike, *Coord. Chem. Rev.* **2001**, *219–221*, 839.
[4] O. Kahn, J. Kröber, C. Jay, *Adv. Mater.* **1992**, *4*, 718.
[5] O. Kahn, C. Jay-Martinez, *Science* **1998**, *279*, 44.
[6] J.-F. Létard, P. Guionneau, E. Codjovi, O. Lavastre, G. Bravic, D. Chasseau, O. Kahn, *J. Am. Chem. Soc.* **1997**, *119*, 10861.
[7] Z. J. Zhong, J. Q. Tao, Z. Yu, C. Y. Dun, Y. J. Liu, X. Z. You, *J. Chem. Soc. Dalton Trans.* **1998**, 327.
[8] S. Hayami, Z. Gu, M. Shiro, Y. Einaga, A. Fujishima, O. Sato, *J. Am. Chem. Soc.* **2000**, *122*, 7126.
[9] L. G. Lavrenova, V. N. Ikorskii, V. A. Varnek, I. M. Oglezneva, S. V. Larionov, *Koord. Khim.* **1986**, *12*, 207.
[10] J. Kröber, J. -P. Audière, R. Claude, E. Codjovi, O. Kahn, J. G. Haasnoot, F. Grolière, C. Jay, A. Bousseksou, J. Linares, F. Varret, A. Gonthier-Vassal, *Chem. Mater.* **1994**, *6*, 1404.
[11] K. H. Sugiyarto, H. A. Goodwin, *Aust. J. Chem.* **1994**, *47*, 263.
[12] R. Bronisz, K. Drabent, P. Polomka, M. F. Rudolf, *Conference Proceedings*, *ICAME95*, **1996**, *50*, 11.
[13] Y. Garcia, P J. van Koningsbruggen, E. Codjovi, R. Lapouyade, O. Kahn, L. Rabardel, *J. Mater. Chem.* **1997**, *7*, 857.
[14] Y. Garcia, P. J. van Koningsbruggen, R. Lapouyade, L. Rabardel, O. Kahn, M. Wierczorek, R. Bronisz, Z. Ciunik, M. F. Rudolf, *C. R. Acad. Sci. Paris* **1998**, *IIc*, 523.
[15] Y. Garcia, P. J. van Koningsbruggen, R. Lapouyade, L. Fournès, L. Rabardel, O. Kahn, V. Ksenofontov, G. Levchenko, P. Gütlich, *Chem. Mater.* **1998**, *10*, 2426.
[16] Y. Garcia, V. Ksenofontov, G. Levchenko, P. Gütlich, *J. Mater. Chem.* **2000**, *10*, 2274.
[17] A. Michalowicz, J. Moscovici, B. Ducourant, D. Cracco, O Kahn, *Chem. Mater.* **1995**, *7*, 1833.
[18] A. Michalowicz, J. Moscovici, O. Kahn, *J. Phys. IV* **1997**, *7*, 633.

  0947-6539/02/0821-4999 $ 20.00+.50/0

[19] Y. Garcia, P. J. van Koningsbruggen, G. Bravic, P. Guionneau, D. Chasseau, G. L. Cascarano, J. Moscovici, K. Lambert, A. Michalowicz, O. Kahn, *Inorg. Chem.* **1997**, *36*, 6357.
[20] N. V. Bausk, S. B. Erenburg, L. G. Lavrenova, L. N. Mazalov, *J. Struct. Chem.* **1994**, *35*, 509.
[21] A. Michalowicz, J. Moscovici, Y. Garcia, O. Kahn, *J. Synchrotron Rad.* **1999**, *6*, 231.
[22] T. Yokoyama, Y Murakami, M. Kiguchi, T. Komatsu, N. Kojima, *Phys. Rev. B* **1998**, *58*, 21.
[23] A. Michalowicz, J. Moscovici, J. Charton, F. Sandid, F. Benamrane, Y. Garcia, *J. Synchrotron Rad.* **2001**, *8*, 701.
[24] M. Verelst, L. Sommier, P. Lecante, A. Mosset, O. Kahn, *Chem. Mater.* **1998**, *10*, 980.
[25] K. Drabent, Z. Ciunik, *Chem. Commun.* **2001**, 1254.
[26] Crystal data for $[Cu(hyptrz)_3](4\text{-chloro-3-nitrophenylsulfonate})_2 \cdot H_2O$ (**4**): $C_{27}H_{35}N_{11}O_{14}S_2Cl_2Cu$, $M_r = 936.2\ g\,mol^{-1}$; blue color; crystal dimensions $0.35 \times 0.25 \times 0.20$ mm; monoclinic, space group $P2_1/c$, $a = 7.9395(3)$, $b = 36.786(2)$, $c = 12.7184(5)$ Å, $\beta = 91.804(3)^\circ$, $V = 3692(1)$ Å^3; $Z = 4$; $\rho_{calcd} = 1.685\ g\,cm^{-3}$. Diffractometer: Nonius Kappa CCD, $Mo_{K\alpha}$ radiation ($\lambda = 0.71069$ Å); $T = 293$ K; $1 < \theta$ range [°] < 22; section of the reciprocal lattice: $0 \le h \le 8$, $0 \le k \le 37$, $-12 \le l \le 12$; of 15026 collected reflections during 5 h; crystal-detector distance of 35 mm; Obs. unique reflections = 3972. Unit-cell parameters were obtained by least-squares refinement from the positions of all the observed reflections in this range. The structure was solved by direct methods with the program MITHRIL.[27] Structure refinement based on F^2 was carried out by extended block-diagonal matrix methods, each block of parameters belonging to a chemical entity such as Cu, hyptrz, $C_6H_3SO_3NO_2Cl$. Locations of hydrogen atoms were generated geometrically (C–H 1.0 Å) and included in the refinement with an isotropic thermal parameter. All non-hydrogen atoms were refined with anisotropic thermal parameters. Neutral atom scattering factors were taken from International Tables for Crystallography.[28] A final difference Fourier map showed residual density of 0.63 e Å^{-3} near Cu locations. Calculations were carried out with programs written or modified locally and illustrations were drawn with ORTEP II[29] and CrystalMaker.[30] $R_{int} = 0.038$; parameters = 657; $R(F) = 0.043$; $wR(F)^2 = 0.111$; $S = 1.01$ with $R(F) = \Sigma\,||F_o| - |F_c||/\Sigma\,|F_o|$ for observed reflections, $wR(F^2) = [\Sigma w F_o^2 - F_c^2)^2/\Sigma w F_o^2]^{1/2}$, $w = 1/(\sigma^2(F^2)) + 0.04\,F^2)$. CCDC-180978 (**4**) contains the supplementary crystallographic data for this paper. These data can be obtained free of charge from the Cambridge Crystallographic Data Centre, 12 Union Road, Cambridge CB2 1EZ, UK; fax: (+44) 1223–336–033; or deposit@ccdc.cam.ac.uk).
[27] C. G. Gilmore, *J. Appl. Crystallogr.* **1984**, *17*, 42.
[28] *International Tables for Crystallography*, *Vol. C*, Tables 4.2.6.8 and 6.1.1.4 (Eds.: A. J. C. Wilson, E. Prince), Kluwer Academic Publishers, **1999**.
[29] C. K. Johnson, *ORTEP*II, Report ORNL-5138. Oak Ridge National Laboratory, Tennessee (USA), **1976**.
[30] D. Palmer, *CrystalMaker 4*, Bicester, Oxfordshire (UK), **1999**.
[31] Y. Garcia, P. Guionneau, G. Bravic, D. Chasseau, O. Kahn, J. A. K. Howard, V. Ksenofontov, S. Reiman, P. Gütlich, *Eur. J. Inorg. Chem.* **2000**, 1531.
[32] P. J. van Koningsbruggen, Y. Garcia, O. Kahn, H. Kooijman, A. L. Spek, J. G. Haasnoot, J. Moscovici, K. Provost, A. Michalowicz, L. Fournès, F. Renz, P. Gütlich, *Inorg. Chem.* **2000**, *39*, 1891.
[33] J. Moscovici, A. Michalowicz, 4th TMR-TOSS-Meeting, Bordeaux, May **2001**.
[34] a) H. Winkler, H. F. Grünsteudel, G. Ritter, R. Lübbers, H.-J. Hesse, G. Nowitzke, G. Wortmann, H. A. Goodwin, *Conference Proceedings*, *ICAME95*, **1996**, *50*, 19; b) R. Lübbers, G. Nowitzke, H. A. Goodwin, G. Wortmann, *J. Phys. IV* **1997**, *7*, 651.
[35] K. H. Sugiyarto, H. A. Goodwin, *Aust. J. Chem.* **1988**, *41*, 1645.
[36] E. Smit, B. Manoun, S. M. C. Verryn, D. de Waal, *Powder Diffr.* **2001**, *16*, 37.
[37] V. Ksenofontov, A. B. Gaspar, J. A. Real, P. Gütlich, **2000**, unpublished results.
[38] W. Vreugdenhil, J. H. van Diemen, R. A. G. de Graaf, J. G. Haasnoot, J. Reedijk, A. M. van der Kraan, O. Kahn, J. Zarembowitch, *Polyhedron* **1990**, *9*, 2971.
[39] E. Codjovi, L. Sommier, O. Kahn, *New J. Chem.* **1996**, *20*, 503.
[40] Y. Garcia, O. Kahn, L. Rabardel, B. Chansou, L. Salmon, J.-P. Tuchagues, *Inorg. Chem.* **1999**, *38*, 4663.
[41] M. Baran, V. Dyanokov, L. Gladczuk, G. Levchenko, S. Piechota, H. Szymczak, *Physica C* **1995**, *241*, 383.
[42] MOSFUN software, Universität Mainz, 1985.
[43] a) A. Michalowicz in *Logiciels pour la Chimie* (Ed.: Société Française de Chimie), Paris, **1991**, 102; b) A. Michalowicz, *J. Phys. IV*, **1997**, *7*, 235.
[44] a) B. K. Teo in *Inorganic Chemistry Concepts*, *EXAFS*: *Basic Principles and Data Analysis*, Springer, Berlin, **1986**, 9; b) D. C. Königsberger, R. Prins, *X-Ray Absorption Principles*, *Applications*, *Techniques of EXAFS*, *SEXAFS and XANES*, John Wiley, New York, **1988**; c) F. W. Lytle, D. E. Sayers, E. A. Stern, *Report of the International Workshop on Standards and Criteria in X-Ray Absorption Spectroscopy*, *Physica* **1989**, *B158*, 701.
[45] B. Lengeler, P. Eisenberger, *Phys. Rev.* **1980**, *B21*, 4507.
[46] a) J. Mustre de Leon, J. J. Rehr, S. I. Zabinsky, R. C. Albers, *Phys. Rev.* **1991**, *B44*, 4146; b) J. J. Rehr, R. C. Albers, *Phys. Rev.* **1990**, *B41*, 8139.
[47] G. Vlaic, D. Andreatta, A. Cepparo, P. E. Cepparo, E. Fonda, A. Michalowicz, *J. Synchr. Rad.* **1999**, *6*, 225.

Received: April 19, 2002 [F4031]